Single-shot spatio-temporal measurements of high-field terahertz pulses

J. van Tilborg*,[1] C. B. Schroeder,[1] Cs. Tóth,[1]

C. G. R. Geddes,[1] E. Esarey,[1,2] and W. P. Leemans[1,2]

[1]*Lawrence Berkeley National Laboratory,*

University of California, Berkeley, California 94720, USA

[2]*University of Nevada, Reno, Nevada 89557, USA*

(Dated: May 29, 2006)

Abstract

The electric field profiles of broad-bandwidth coherent terahertz (THz) pulses, emitted by laser-wakefield-accelerated electron bunches, are studied. The near-single-cycle THz pulses are measured with two single-shot techniques in the temporal and spatial domains. Spectra of $0-6$ THz and peak fields up to $\simeq$0.4 MV cm^{-1} are observed. The measured field substructure demonstrates the manifestation of spatio-temporal coupling at focus, which affects the interpretation of THz radiation as a bunch diagnostic and in high-field pump-probe experiments. A ray-based model confirms the coupling.

PACS numbers: 41.60.-m, 52.38.Kd, 78.47.+p, 07.57.Hm

* Also at Eindhoven University of Technology, the Netherlands.

Intense THz radiation, covering electro-magnetic wavelengths of 10–1000 μm, is interesting for studies of ultra-fast processes in semi- and superconductors [1–5]. Peak THz fields on the order of MV cm^{-1} allow for use of the THz pulse as the pump beam in pump-probe experiments. While conventional laser-based sources (e.g. optical rectification or the photoconductive antenna) are typically limited to generation of $\lesssim$ 50 kV cm^{-1} fields, coherent THz emission from femtosecond electron bunches has been described to yield single-cycle radiation that is potentially 1–2 orders of magnitude more intense [6–10]. The coherent THz radiation from such sources is also used as a diagnostic for the temporal charge profile of the electron bunch. The results described in this Letter are based on THz emission from electron bunches produced by a laser wakefield accelerator (LWFA) [11, 12]. The LWFA delivers multi-nanocoulomb relativistic electron bunches, intrinsically synchronized to the laser pulse. Through emission of coherent transition radiation (CTR) [13], these ultra-short bunches emit THz pulses as they exit the plasma-vacuum boundary [7, 8, 10, 14, 15].

Studies of spatio-temporal coupling of the THz fields at focus have been performed with scanning techniques on conventional low-field laser-based THz sources [16–19]. Here we report on single-shot measurements of the temporal and spatial profiles of intense LWFA-produced THz pulses, which have applications in high-field THz experiments and as an electron bunch diagnostic. For both these applications, the spatio-temporal coupling impacts the temporal properties of the radiation pulse and, therefore, the interpretation of experimental results. In addition, due to shot-to-shot fluctuations in the LWFA performance, development of single-shot techniques are required. A two-dimensional (2D) spatial technique, reported by Wu *et al.* [20], and a single-shot temporal technique, reported for measurement of self-fields of an electron bunch [21], have been implemented. The results in this Letter also demonstrate the first direct single-shot temporal measurement of a THz pulse field profile. These measurements reveal the high-field nature of the LWFA-produced THz pulses ($\simeq$0.4 MV cm^{-1}), which are found to have a near-single-cycle field profile.

The high-power Ti:Al_2O_3 laser of the LOASIS facility [22] at the Lawrence Berkeley National Laboratory was used for the experiments. Two variations of the EOS technique were operated to characterize the THz pulses, namely a single-shot temporal cross-correletation technique [21] and a single-shot two-dimensional (2D) spatial technique [20]. As depicted in Fig. 1, a Ti:Al_2O_3 laser beam (wavelength of λ_0 = 800 nm) was focused by an off-axis parabola (OAP1) to a spot size of $\simeq$ 3.6 μm [root-mean-square (rms)]. From a supersonic

gas jet (diameter of 2 mm), Helium gas was emanated. Through the nonlinear laser-plasma interaction (plasma electron density of 3×10^{19} cm^{-3}), an electron bunch with a total charge of $\simeq 2$ nC was produced. The electron energy distribution $g(E)$ was measured to be of the form $g(E) \propto \exp(-E/E_t)$, with $E_t = 5$ MeV. THz radiation was emitted as the electrons propagated through the dielectric discontinuity of the plasma-vacuum boundary [7, 8, 10, 14].

An F/2 90°-off-axis parabola (OAP2, 15 cm focal length), positioned off-centered ($\theta = 19°$ with respect to the main propagation axis), was used to collect and collimate a portion of the emitted THz radiation. The collimated THz radiation was focused by an F/2.4 90°-off-axis parabola (OAP3, 18 cm focal length) onto a 200-μm-thick GaP crystal, positioned outside the target chamber. A 3.2-mm-thick polyethylene (PE) disk served as window. For THz pulses in the $0-8$ THz regime, PE has a negligible contribution to pulse reshaping.

For the single-shot temporal EOS technique, two laser beams, both with a minimum pulse length of 70 fs [intensity full-width-at-half-maximum (FWHM)], were split off from the main laser beam, conserving synchronization. The delay between both probe beams with respect to the THz pulse was varied with a delay stage. The compressor of the the first probe beam, $I_1(t)$ in Fig. 1, was deliberately detuned to provide a chirped laser pulse with a length of 1350 fs (intensity FWHM). After propagation through a polarizer, defining a pure horizontal polarization state, the laser pulse was focused (spotsize < 20 μm) to overlap with the THz beam in the GaP crystal. A $\lambda/4$ plate was rotated to yield a circular polarization state incident on the analyzer, which transmitted only the vertical polarization. The GaP crystal was cut in the $\langle 110\rangle$ plane, and its $\langle 001\rangle$ axis was rotated to optimize the electro-optic (EO) effect. Although the emitted THz pulse was radially polarized coming from the plasma-vacuum boundary [8], OAP2 selected a specific polarization component which corresponded to vertical polarization at the GaP surface.

Through the THz-induced EO effect in the GaP crystal, the intensity envelope of the analyzer transmission of probe laser $I_1(t)$ (originally circularly polarized) is modulated to $I_m(t)$. It can be shown [23] that $I_m(t) = \frac{1}{2}\left[1+\sin\Gamma^*(t)\right] I_1(t)$, where in the Fourier domain $\Gamma^*(\nu) = \Gamma_{\rm THz}(\nu) T_{\rm GaP}(\nu)$ and ν the radiation frequency. $\Gamma^*(\nu)$ represents the THz-induced phase retardation and $T_{\rm GaP}(\nu)$ incorporates GaP crystal effects [23, 24] such as absorption, dispersion, velocity mismatch between the laser and THz pulse, and surface reflections. The function $T_{\rm GaP}(\nu)$ for 200-μm-thick GaP was discussed in Ref. [15]: over the frequency range 0-8 THz effects of dispersion were found to be relatively limited. The THz retardation

function $\Gamma_{\mathrm{THz}}(t)$ is related to the original THz field profile $E_{\mathrm{THz}}(t)$ through [24, 25]

$$\Gamma_{\mathrm{THz}}(t) = 2\pi L n_0^3 r_{41} E_{\mathrm{THz}}(t)/\lambda_0, \tag{1}$$

with $L = 200$ μm the GaP crystal length, $n_0 = 3.19$ the index of refraction in GaP at λ_0, and $r_{41} \simeq 2 \times 10^{-12}$ m V^{-1} the EO coefficient of GaP [26]. The THz field $E_{\mathrm{THz}}(\nu)$ is determined by the Fourier transformation of the electron bunch charge profile $Q(t)$ and diffraction effects $D(\nu)$ from the limited size of the transverse plasma-vacuum interface [8, 14, 15].

The EO-modulated laser envelope was recorded in a single-shot manner [21] through non-collinear sum-frequency generation of $I_m(t)$ and a second short laser pulse $I_2(t - \tau_2)$ (pulse length of $\sigma_2 = 70$ fs intensity FWHM), with τ_2 the respective temporal delay between both laser beams. The frequency doubling occurred in a beta barium borate (BBO) crystal. A CCD camera (CCD 1), see Fig. 1, recorded the time-integrated transverse (xy plane) intensity distribution of the frequency-doubled radiation $I_{2\omega}(x, y)$. During post-processing, each image $I_{2\omega}(x, y)$ was integrated over x to yield $I_{2\omega}(y)$. Also, each profile was normalized to yield $I_{2\omega} \rightarrow (I_{2\omega} - I_{2\omega,0})/I_{2\omega,0}$, with $I_{2\omega,0}$ the reference profile in absence of a THz pulse. Due to the non-collinear geometry, the delay τ_2 is a function of the position y within the crystal and $I_{2\omega}(y)$ can be converted to a temporal profile $I_{2\omega}(\tau_2)$ through $\tau_2 = (y/c)\tan(\alpha^*/2)$, with c the speed of light in vacuum. The angle of incidence between both laser pulses at the crystal surface was $\alpha = 10^\circ$ (inside the BBO crystal $\alpha^* = 6.3^\circ$), and the laser beam diameters were $\simeq 6$ mm (intensity FWHM). After defining a measured retardation function $\Gamma_{\mathrm{cor}}(\tau_2)$ as $\Gamma_{\mathrm{cor}}(\tau_2) = \arcsin I_{2\omega}(\tau_2)$, it can be found [23, 24] that

$$\Gamma_{\mathrm{cor}}(\nu) \simeq \Gamma_{\mathrm{THz}}(\nu) T_{\mathrm{GaP}}(\nu) I_{\mathrm{env},2}(\nu), \tag{2}$$

with $I_{\mathrm{env},2}(\nu)$ the Fourier transformation of the envelope of $I_2(t)$. This latter expression is exact in either the limit $\Gamma_{\mathrm{cor}} \ll 1$ rad or $\sigma_2 \rightarrow 0$ fs, and is less than 4% off for the parameters $\Gamma_{\mathrm{cor}} = 1$ rad and $\sigma_2 = 70$ fs.

In order to measure single-shot 2D-spatial THz images, the setup in Fig. 1 was slightly modified. The $\lambda/4$ plate was rotated to conserve the linear polarization and the two lenses in the path of probe laser 1 were removed, such that a collimated laser beam was overfilling the THz spot at the GaP surface. By removing the flipper-mirror, the 2D time-integrated intensity distribution $I_{2D}(x, y, \tau)$ was recorded by CCD camera 2, with τ the delay between $E_{\mathrm{THz}}(t)$ and $I_1(t)$. The compressor for probe laser 1 was tuned to yield a pulse length of 70

fs (intensity FWHM), which allowed for time-resolved 2D imaging. For a linear-polarized laser beam, it can be derived [23, 24] that $I_{2D}(x, y, \tau) \propto \int I_1(t-\tau) \sin^2 [\Gamma^*(x, y, t)/2] dt$, with $\Gamma^*(\nu)$ previously defined in the Fourier domain.

Three measured representative phase retardation profiles $\Gamma_{\rm cor}(t)$ and $|\Gamma_{\rm cor}(\nu)|$, obtained through the single-shot temporal EOS measurement of $I_{2\omega}(\tau_2)$, are shown in Fig. 2(a) and 2(b), respectively. Shot A in Fig. 2(a) shows a field profile with just one main field cycle (spectrum extending to $\simeq 6$ THz) and peak phase retardation of $\Gamma_{\rm cor} \simeq 1$ rad. By combining Eqs. (1) and (2), and considering that the field reducing effects of dispersion and surface transmission in the GaP crystal can be approximated as $\times \frac{1}{4}$ [15], an estimation of the THz field amplitude at the crystal location yields $E_{\rm THz} \simeq 0.4$ MV cm^{-1}.

The shots of Fig. 2 also display the presence of a second (trailing) THz pulse (two maxima in the temporal domain and interference in the spectral domain). Although the position of the trailing pulse was relatively stable at a delay of $230 - 250$ fs, its relative field strength showed a stronger fluctuation (from weak in shot A to stronger in shot C). Each measurement (in the time and frequency domain) was compared to a modeled EOS profile. The model was based on a 45 fs (rms) electron bunch and the emission of two THz pulses at a separation of 240 fs. The transverse size of the plasma was set at $\rho = 150$ μm (based on plasma density interferometry) and the electron energy at $E_t = 5$ MeV. The relative field amplitude of the trailing pulse was 30%, 57%, and 90% for shots A, B, and C, respectively.

After switching the setup to the single-shot 2D EOS technique, the 2D laser transmission $I_{2D}(x, y, \tau)$ was recorded while varying the delay τ between the laser and THz beam. It was found that the 2D THz profile was stable at a given delay, but evolved over time. Three characteristic $I_{\rm 2D}(x, y, \tau)$ images are shown in Figs. 3(a)–(c), with (a) $\tau = -250$ fs, (b) $\tau = 0$ fs, and (c) $\tau = 350$ fs. The data shows that a main THz spot is present, see for example Fig. 3(b), where the main spot has an intensity FWHM of $\simeq 600$ μm. The substructure indicates the presence of effects from diffraction [e.g. shot D in Fig. 3(a)], coma [e.g. shot F in Fig. 3(c)], and other aberrations [27]. Diffraction is present since the THz emission overfills parabola OAP2 (see Fig. 1), while coma can be present if the alignment of OAP2 and OAP3 is not perfect. At a fixed delay $\tau = 0$ fs, yet another three consecutive images were analyzed by taking a lineout at $y = 0$ mm. The three lineouts, shown in Fig. 3(d), indicate that the position of the substructure is stable, but that the relative intensity fluctuates shot-to-shot.

Through detailed studies of the LWFA performance, it was found that it is unlikely that the double-THz-pulse structure (*e.g.* EOS measurements in Fig. 2) is a result of the LWFA production of two electron bunches, but rather the result of optical effects in the THz radiation focusing system (diffraction, coma, and other aberrations). To model the focal properties of the THz pulse, a 1D transverse ray-based model was developed. Consider a collection of optical rays, each reflected off a 90°-off-axis parabola. In the frame of each ray (with z the direction of propagation), the normalized field profile is defined as

$$E(r,z,t) = \left[1 - \frac{(t-\frac{z}{c})^2}{\sigma_t^2}\right] \exp\left[-\frac{(t-\frac{z}{c})^2}{2\sigma_t^2}\right] \exp\left[-\frac{r^2}{\sigma_r^2}\right], \tag{3}$$

with σ_r and σ_t the transverse and longitudinal pulse size respectively. Note that the pulse profile in Eq. (3) is based on THz radiation emitted by ultra-relativistic electrons propagating through a metal-vacuum boundary [14, 15]. By rotating the parabola by 0.4 rad, coma was induced. The field profiles $E(r,z)$ at consecutive time steps are shown in Fig. 4(a). One can see that transverse and longitudinal substructure is present at the focal volume, induced by the coma. At the fixed location $r/\sigma_r = -1$ and $z = 0$, the temporal field profile $E(t)$ is shown in Fig. 4(b), with the Fourier transformation $|E(\nu)|$ in Fig. 4(c). The double-pulse profile is clearly present, including spectral interference. The temporal pulse separation is a function of the location (r,z). For comparison, the profiles $E(t)$ and $|E(\nu)|$ at the center of the focal point for the case of no coma are shown in Fig. 4(d) and Fig. 4(e), respectively.

The parameters for the ray-based model were not chosen to match the EOS experiments in detail. Effects such as a frequency dependent Rayleigh range, the Gouy phase shift, and bandwidth-induced dispersion at focus, [17, 28, 29] have not been included. However, the model does indicate that through coma (or diffraction and other aberrations), the field profile is subject to spatio-temporal coupling. The model shows a temporal double-field profile at focus, which already resembles the experimental observations. Experimentally, the spatio-temporal coupling is fixed by the arrangement and alignment of the optics in the THz beam line, resulting in a stable positioning of the temporal and spatial substructure (c.f. Figs. 2 and 3). However, fluctuations of the electron bunch energy and pointing can result in a varying angular THz emission profile, which in return yield fluctuations in the amplitude ratio of the field structure.

In summary, two single-shot techniques allowed for studies of spatio-temporal properties of single-cycle broad-bandwidth THz pulses at focus. The temporal EOS technique showed

THz pulses with spectra of $0-6$ THz and peak fields of $\simeq$0.4 MV cm^{-1}. Through comparison with a CTR-based model, the electron bunches were found to have a duration of $\simeq$ 45 fs. A trailing THz pulse, with varying amplitude, was observed at a stable separation of $\simeq$ 240 fs. A 2D-spatial EOS technique indicated the presence of a main THz spot surrounded by time-evolving substructure. Both techniques, in combination with a ray-based model, support the conclusion that diffraction, coma, and other aberrations, are spatio-temporally coupled in the focal volume.

The authors acknowledge contributions from R. Huber and R. Kaindl on EOS. This work was supported by the Director, Office of Science, Office of High Energy Physics, of the U.S. Department of Energy under Contract No. DE-AC02-05CH11231.

[1] T.-I. Jeon and D. Grischkowsky, Phys. Rev. Let. **78**, 1106 (1997).

[2] K. B. Nordstrom *et al.*, Phys. Rev. Lett. **81**, 457 (1998).

[3] J. Orenstein and A. J. Millis, Science **288**, 468 (2000).

[4] R. A. Kaindl *et al.*, Nature **423**, 734 (2003).

[5] R. Huber *et al.*, Phys. Rev. Lett. **96**, 017402 (2006).

[6] G. L. Carr *et al.*, Nature **420**, 153 (2002).

[7] W. P. Leemans *et al.*, Phys. Rev. Lett. **91**, 074802 (2003).

[8] C. B. Schroeder *et al.*, Phys. Rev. E **69**, 016501 (2004).

[9] A. L. Cavalieri *et al.*, Phys. Rev. Lett. **94**, 114801 (2005).

[10] J. van Tilborg *et al.*, Phys. Rev. Lett. **96**, 014801 (2006).

[11] T. Tajima and J. M. Dawson, Phys. Rev. Lett. **43**, 267 (1979).

[12] E. Esarey *et al.*, IEEE Trans. Plasma Sci. **24**, 252 (1996).

[13] M. L. Ter-Mikaelian, *High-energy electromagnetic processes in condensed media* (Wiley, New York, 1972).

[14] J. van Tilborg *et al.*, Laser Part. Beams **22**, 415 (2004).

[15] J. van Tilborg *et al.*, Phys. Plasmas **13**, in press (2006).

[16] M. Kempe and W. Rudolph, Phys. Rev. A **48**, 4721 (1993).

[17] M. A. Porras, Phys. Rev. E **65**, 026606 (2002).

[18] S. Hunsche *et al.*, J. Opt. Soc. Am. A **16**, 2025 (1999).

[19] Zhiping Jiang *et al.*, Appl. Phys. Lett. **74**, 1191 (1999).

[20] Q. Wu, T. D. Hewitt, and X.-C. Zhang, Appl. Phys. Lett. **69**, 1026 (1996).

[21] S. P. Jamison *et al.*, Opt. Lett. **28**, 1710 (2003).

[22] W. P. Leemans *et al.*, Phys. Plasmas **11**, 2899 (2004).

[23] G. Gallot and D. Grischkowsky, J. Opt. Soc. Am. B **16**, 1204 (1999).

[24] J. Faure *et al.*, Opt. Quantum Electron. **36**, 681 (2004).

[25] Q. Chen *et al.*, J. Opt. Soc. Am. B **18**, 823 (2001).

[26] Q. Wu and X.-C. Zhang, Appl. Phys. Lett. **70**, 1784 (1997).

[27] M. Born and E. Wolf, *Principles of Optics* (Pergamom Press, Oxford, 1980).

[28] D. You and P. H. Bucksbaum, J. Opt. Soc. Am. B **14**, 1651 (1997).

[29] S. Feng, H. G. Winful, and R. W. Hellwarth, Opt. Lett. **23**, 385 (1998).

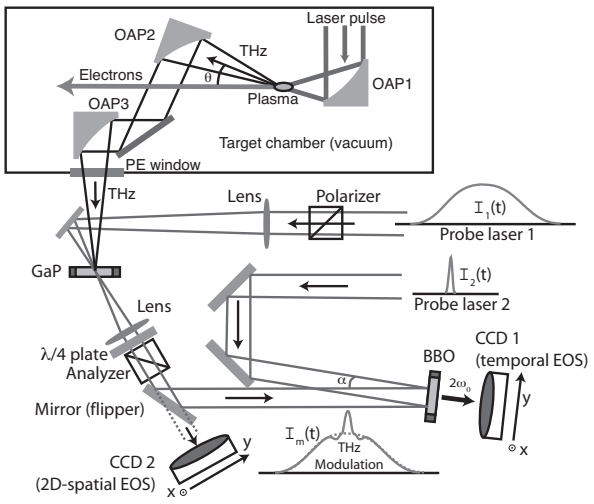

FIG. 1: Schematic representation of the laser-wakefield accelerator (LWFA), the THz (CTR) beam path, and the two EOS detection setups (temporal and 2D-spatial).

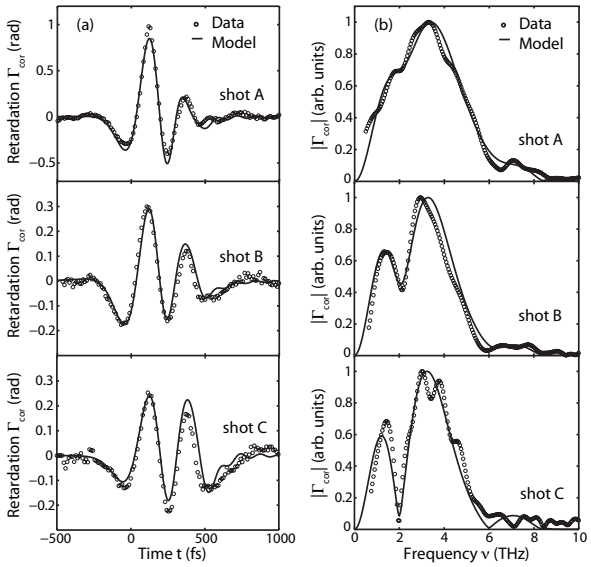

FIG. 2: (a) Measured single-shot THz field profiles in terms of phase retardation $\Gamma_{\rm cor}(t)$. (b) Fourier transformation $|\Gamma_{\rm cor}(\nu)|$ of the data. The solid curves are calculated from a model based on CTR from a 45 fs (rms) electron bunch, while considering the emission of two THz pulses (separation of 240 fs and varying amplitude ratio).

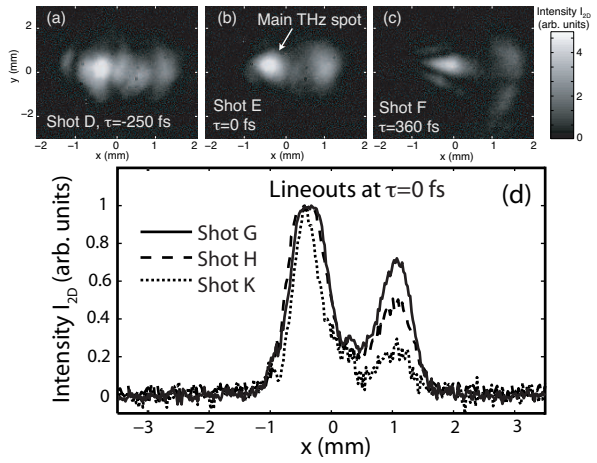

FIG. 3: Three characteristic single-shot 2D THz images $I_{2D}(x, y, \tau)$, taken at different values for the delay between the THz and laser pulse: (a) $\tau = -250$ fs, (b) $\tau = 0$ fs, and (c) $\tau = 350$ fs. At a fixed delay $\tau = 0$ fs, lineouts at $y = 0$ of three consecutive shots are displayed in (d).

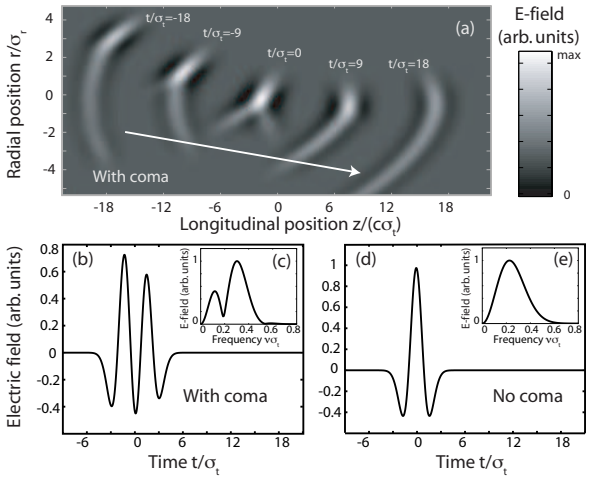

FIG. 4: (a) Evolution the simulated field profile $E(r, z)$ at various time steps. The 90°-off-axis parabola was rotated by 0.4 rad (coma). With coma present, the temporal field profile $E(t)$ at a fixed location $r/\sigma_r = -1$ and $z = 0$ is shown in (b), with the Fourier transformation $|E(\nu)|$ in (c). For comparison, without coma present, the field profiles $E(t)$ and $|E(\nu)|$ at the center of the focal spot are shown in (d) and (e), respectively.